# Highlights

- Neural trajectories in the hippocampus exhibited greater variability during a working memory (WM) task compared to those in the entorhinal cortex and amygdala regions.

- The distance of neural trajectories between encoding and retrieval states in the hippocampus was memory-load dependent during a WM task.

- Hippocampal neural trajectories fluctuated between the encoding and retrieval states in a task-dependent manner during both baseline and sharp-wave ripple (SWR) periods.

- Hippocampal neural trajectories shifted from encoding to retrieval states during SWR period.

# Hippocampal neural fluctuations between memory encoding and retrieval states during a working memory task in humans

Yusuke Watanabe[a,*], Yuji Ikegaya[b,c,d], Takufumi Yanagisawa[a,e]

[a]*Institute for Advanced Cocreation studies, Osaka University, 2-2 Yamadaoka, Suita, 565-0871, Osaka, Japan*
[b]*Graduate School of Pharmaceutical Sciences, The University of Tokyo, 7-3-1 Hongo, Tokyo, 113-0033, Japan*
[c]*Institute for AI and Beyond, The University of Tokyo, 7-3-1 Hongo, Tokyo, 113-0033, Japan*
[d]*Center for Information and Neural Networks, National Institute of Information and Communications Technology, 1-4 Yamadaoka, Suita City, 565-0871, Osaka, Japan*
[e]*Department of Neurosurgery, Osaka University Graduate School of Medicine, 2-2 Yamadaoka, Osaka, 565-0871, Japan*

**Abstract**

Working memory (WM) ~~, critical to various~~ is fundamental to a plethora of cognitive functions, ~~embodies~~ but the intricate neural mechanisms ~~which are not entirely understood. Notably, the role~~ crucial to its operation are not fully comprehended. In particular, the roles of the hippocampus and sharp-wave ripple complexes (SWRs) ~~– coordinated, rapidneuronal —~~ rapid, synchronised neural events within the hippocampus ~~– in WM tasks remains somewhat ambiguous, notwithstanding their confirmed involvement in —~~ are known to facilitate memory consolidation and retrieval~~. In our present research, we posit that multiunit activity patterns within the hippocampus operate synergistically~~ , yet their contributions to WM tasks remain somewhat ambiguous. We propose that the coordinated activity patterns in the hippocampus work in unison with SWRs, ~~consequently exhibiting distinctive~~ displaying distinct dynamics during WM tasks. Our study ~~engaged in a comprehensive~~ involved an extensive analysis of a dataset ~~derived~~ obtained from intracranial electroencephalogram recordings from the medial temporal ~~lobes~~ lobe (MTL) of nine epileptic patients ~~executing~~ during an eight-second Sternberg task. We utilised Gaussian-process factor analysis ~~was utilized to pinpoint~~ to identify low-dimensional neural ~~vectors~~representations, or 'trajectories,' within the MTL areas during the WM task. We ~~discovered that the hippocampus showed the most pronounced variation in neural trajectories relative~~ found that the neural trajectory displayed the most substantial variations in the hippocampus compared to the entorhinal cortex and ~~the amygdala. Intriguingly,~~ amygdala. Moreover, we observed that the deviation in trajectories between ~~the~~ encoding and retrieval phases was ~~seen to be~~ dependent on memory load. ~~Further~~Interestingly, hippocampal trajectories ~~showed oscillatory behavior~~ oscillated during the retrieval phase, ~~indicating task-related transitions~~ revealing task-dependent shifts between encoding and retrieval states, ~~and embracing both~~ which encompassed baseline and SWR ~~episodes~~phases. These oscillations transitioned from encoding to retrieval states ~~in correlation with the SWRs. Hence, these findings underscore the crucial~~ consistent with the occurrence of SWRs. These findings underline the significant role of the hippocampus ~~in tackling~~ during the performance of WM tasks and ~~propose an enticing hypothesis for future~~ put forward a compelling hypothesis for further exploration: the ~~functional state of the hippocampus switches~~ hippocampus undergoes a functional transition from encoding to retrieval during SWRs.

*Keywords:* working memory, WM, memory load, hippocampus, sharp-wave ripples, SWR, humans

Working memory (WM) ~~serves a critical~~ plays a crucial role in everyday life, ~~with its neural foundations being an ongoing subject of study~~and its neural underpinnings remain an area of ongoing research. The hippocampus, ~~particularly crucial to memoryfunction, remains central to this research~~ notably integral to memory, continues to be a primary focus of this investigation [1] [2] [3] [4] [5] [6] [7] [8] [9]. ~~Understanding~~ Gaining insights into the role

*Corresponding author. Tel: +81-6-6879-3652

of the hippocampus in working memory is ~~essential to advancing our comprehension~~ vital to deepening our understanding of cognitive processes, ~~thereby promoting~~ hence fostering the progression of cognitive training and interventions.

Current evidence ~~points toward a brief~~suggests a transient, synchronized oscillation, ~~known~~ referred to as sharp-wave ripple (SWR) [10], ~~being associated~~ is linked with several cognitive functions~~. These include~~, such as memory replay [11] [12] [13] [14] [15], memory consolidation [16] [17] [18] [19], memory recall [20] [21] [22], and neural plasticity [23] [24]. This ~~suggests that SWR may play a crucial part in~~ evidence indicates the likelihood that SWR could be a critical component of hippocampal processing, contributing to ~~the performance of working memory~~ working memory performance. However, ~~studies~~ research investigating the effects of SWRs on working memory ~~are limited [25]and focus primarily on rodent models engaged~~ remains sparse [25], and is largely limited to rodent models participating in navigation tasks ~~, without clear delineation~~ where the timing of memory acquisition and recall ~~timing~~is not explicitly distinguished.

Recent studies ~~have illustrated~~ indicate that hippocampal neurons ~~present~~ exhibit low-dimensional representations during WM tasks. ~~Specifically~~Notably, the firing patterns of place cells [26] [27] [28] [29] [30], located in the hippocampus, ~~appear~~ are observed to be encompassed within a dynamic, nonlinear three-dimensional hyperbolic geometry in ~~rodent models [31] . Additionally~~rodents [31]. Moreover, grid cells in the entorhinal cortex (EC)—the ~~main route~~ dominant pathway to the hippocampus [32] [33] [34]—~~display a~~ displayed toroidal topology during exploration [35]. ~~Regrettably, these studies are limited~~ Unfortunately, these investigations are confined to spatial navigation tasks in rodents, ~~affecting~~ thus imposing limitations on the temporal resolution of WM tasks. The ~~application~~ applicability of these findings to human subjects and their ~~extension~~ generalization beyond navigation tasks ~~are still unconfirmed~~remains to be established.

~~In light of these points, the present study seeks to corroborate~~ Given these considerations, the current study aims to validate the hypothesis that hippocampal neurons ~~portray unique~~ exhibit distinctive representations in low-dimensional spaces, ~~referred to~~ designated as 'neural trajectory,' ~~particularly during SWR periods in WM tasks. To test this proposition, we used a dataset from~~ during WM tasks, most prominently within SWR periods. To evaluate this claim, we employed a dataset of patients performing an eight-second Sternberg task with high temporal resolution (1 ~~second~~ s for fixation, 2 ~~seconds~~ s for encoding, 3 ~~seconds~~ s for maintenance, and 2 ~~seconds~~ s for retrieval)~~with a high temporal resolution~~, while their intracranial electroencephalography signals (iEEG) ~~signals in~~ within the medial temporal lobe (MTL) were being monitored [36]. To ~~explore the~~ investigate low-dimensional neural trajectories, we ~~utilized the~~ employed Gaussian-process factor analysis (GPFA), a ~~recognized technique for examining~~ method renowned for analyzing neural population dynamics [37].

## 1. Methods

### *1.1. Dataset*

A ~~public dataset [36] comprising experiments from~~ publicly available dataset [36] was used, which consists of nine epilepsy patients ~~was taken into consideration for this study. The patients were tasked with executing~~ performing a modified Sternberg task~~which included~~. This task involves four phases: fixation (1s), encoding (2s), maintenance (3s), and retrieval (2s) [36]. During the encoding phase, participants were ~~presented with~~ exposed to four, six, or eight alphabet letters, ~~known~~ referred to as the set size. Subsequently, they had to ~~ascertain~~ decide whether a probe letter ~~revealed~~ presented during the retrieval phase was ~~displayed earlier (the suitable~~ previously displayed (the correct choice for the Match IN task) or not (the ~~suitable~~ correct choice for the Mismatch OUT task). iEEG signals were ~~registered via~~ recorded at a sampling rate of 32 kHz, within a frequency ~~spectrum~~ range of 0.5–5,000 Hz, ~~utilizing~~ using depth electrodes implanted in the medial temporal lobe (MTL) regions: the anterior head of the left and the right hippocampus (AHL and AHR), the posterior body of the hippocampus (PHL and PHR), the entorhinal cortex (ECL and ECR), and the amygdala (AL and AR)~~(~~, as illustrated in Figure 1A and Table 1~~). The recorded~~ . The iEEG signals were subsequently downsampled to a rate of 2 kHz. ~~The interrelationship~~ Correlations among variables such as set size and correct rate were ~~explored~~ investigated (Figure **??**S1). The timings of multiunit spikes were

identified using determined by a spike sorting algorithm [38] with using the Combinato package (`https://github.com/jniediek/combinato`)(Figure 1C).

### 1.2. Calculation of neural trajectories using GPFA

Neural trajectories, colloquially called also termed 'factors' (Figure 1D), in the hippocampus, EC, and amygdala (Figure 1D)were calculated utilizing GPFA [37] , which was , were computed using GPFA [37] applied to the multiunit activity data radiating from for each session. The computations were GPFA was performed with the elephant package (`https://elephant.readthedocs.io/en/latest/reference/gpfa.html`). The bin size was set at to 50 ms, with no overlaps. Each factor was z-normalized across all sessions. The Euclidean distance from the origin ($O$) was subsequently then calculated (Figure 1E).

For each trajectory inside within a region, for exampleinstance, AHL, *geometric medians* (i.e., $g_F$ for fixation, $g_E$ for encoding, $g_M$ for maintenance, and $g_R$ for retrieval phase) were calculated by finding determined by calculating the median coordinates of the trajectory during the four phases (Figure 1D). An optimal dimensionality for GPFA was identified as three using the elbow method, which was derived by investigating the log-likelihood values through a three-fold cross-validation technique approach (Figure 2B).

### 1.3. Identifying SWR candidates from areas of the hippocampushippocampal regions

Potential SWR instances from events within the hippocampus were identified via an detected using a widely accepted method [39]. LFP signals from a given region of interest (ROI), such as AHL, were re-referenced by subtracting a calculated average an averaged signal from locations outside the ROI (e.g.*e.g.*, AHR, PHL, PHR, ECL, ECR, AL, and AR) (see Figure 1A). The re-referenced LFP signals were further then filtered with a ripple-band filter (80–140 Hz) to detect identify SWR candidates (=$SWR^+$ candidates) (see Figure 1B). SWR detection was carried out conducted using a published tool (`https://github.com/Eden-Kramer-Lab/ripple_detection`) [40], with the bandpass range adjusted to 80–140 Hz in line with human requirements for humans [21] [22], as opposed to the conventional different from the original 150–250 Hz range typically applied to rodents.

Control events for $SWR^+$ candidates, tagged labeled as $SWR^-$ candidates, were identified by randomly shuffling the timestamps of $SWR^+$ candidates randomly across all trials and subjects. The resultant resulting $SWR^+/SWR^-$ candidates underwent visual inspection(were then subjected to visual inspection, as shown in Figure 1).

### 1.4. Defining SWRs from alleged putative hippocampal CA1 regions

SWRs were distinguished from SWR candidates within likely in presumptive CA1 regions. Initially, these regions were designated defined as follows: $SWR^+/SWR^-$ candidates from in the hippocampus were mapped projected into a two-dimensional space based on the overlapping spike counts per unit using a supervised employing a supervised method using UMAP (Uniform Manifold Approximation and Projection) [41] (Figure 4A). Validation of the clustering was done Clustering validation was performed by computing the silhouette score [42] from the clustered samples (Table 2). Those areas Regions in the hippocampusscoring over , which scored above 0.6 on average across sessions (or the 75th percentile) were specified as likely (Figure 4B), were characterized as presumed CA1 regions, in turn, identifying five electrode positions across five participants from five patients (Table 3).

Those $SWR^+/SWR^-$ candidates within in the assumed CA1 regions were classified as $SWR^+/SWR^-$and had , thus relinquishing their candidate statusrevoked. Log-normal distributions were observed in the . The duration and ripple band peak amplitude of SWRs were observed to follow log-normal distributions (Figure 44C & E). Each SWR time period time period of SWR was partitioned relative to the time from the SWR center into pre- (at −800 to −300 ms from SWR center), mid- (at −250 to +250 ms), and post- post-SWR (at +300 to +800 ms) SWR times.

### 1.5. Statistical evaluation

The Brunner–Munzel test and the Kruskal-Wallis test were performed using the SciPy package in Python [43]. A correlation analysis was executed Correlational analysis was performed by determining the rank of the

observed correlation coefficient in its associated set-size-shuffled surrogate using a custom Python script. The bootstrap test was ~~conducted with~~ implemented using an in-house Python script.

## 2. Results

### 2.1. *iEEG recording and neural trajectory in MTL regions during a Sternberg task*

We ~~analyzed~~ leveraged a publicly available dataset for this ~~study~~ analysis [36]. This dataset ~~consists of~~ encompasses LFP signals (Figure 1A) from MTL regions (Table 1) ~~obtained~~ during a modified Sternberg task ~~performance~~execution. We identified $SWR^{+}$ candidates from LFP signals filtered through the 80–140 Hz ripple band (Figure 1B), originating across all hippocampal regions (refer to Methods). Correspondingly, $SWR^{-}$ candidates were defined at ~~the same timestampsbut shuffled between~~ identical timestamps) but shuffled across different trials (Figure 1). The dataset included multiunit spikes (Figure 1C) identified via a spike sorting algorithm [38]. ~~Using~~ By employing GPFA [37], and using the 50-ms binned multiunit activity ~~without~~ with no overlaps, we determined the neural trajectories (or factors) of MTL regions ~~per~~ by session and region (Figure 1D). We normalized each factor by session and region ~~,~~ for instance, session #2 in AHL of subject #1. Subsequently, we calculated the Euclidean distance from the origin ($O$) (Figure 1E).

### 2.2. ~~*Correlation between hippocampal*~~ *Hippocampal neural trajectory* ~~*and*~~ *correlation with a Sternberg task*~~*performance*~~

Figure 2A ~~shows~~ illustrates the cloud of median neural trajectories of 50 trials within the three main factor spaces. We determined the optimal embedding dimension for the GPFA model to be three, using the elbow method (Figure 2B). The trajectory distance from the origin ($O$) (represented as $\|g_F\|$, $\|g_E\|$, $\|g_M\|$, and $\|g_R\|$) in the hippocampus ~~was greater than the~~ exceeded corresponding distances in the EC and amygdala (Figures 2C and D).[1]

Similarly, we ~~calculated~~ computed the distances between the geometric medians of ~~the~~ four phases, namely $\|g_F g_E\|$, $\|g_F g_M\|$, $\|g_F g_R\|$, $\|g_E g_M\|$, $\|g_E g_R\|$, and $\|g_M g_R\|$. The results indicated that the hippocampus ~~showed~~ displayed larger distances between phases than both the EC and amygdala. [2]

### 2.3. *Memory* ~~*load-dependence of*~~ *load-dependent neural trajectory distance between encoding and retrieval states in the hippocampus*

In ~~the context~~ terms of memory load in the ~~Sternberg~~ Stenberg task, we ~~found~~ identified a negative correlation between the correct rate of trials and set size (the number of letters to encode) (Figure 3A).[3] Similarly, ~~we observed~~ a positive correlation was observed between the response time and set size (Figure 3B).[4].

~~Additionally, we observed~~ Furthermore, we found a positive correlation between set size and the trajectory distance between the encoding and retrieval phases ($\log_{10}\|g_E g_R\|$) (Figure 3C).[5]. However, ~~the~~ distances between other combinations of phases did not ~~show~~ display statistically significant correlations (Figures 3D and S2).

### 2.4. *Detection of hippocampal SWR from putative CA1 regions*

~~To better localize~~ For precision improvement in recording sites and ~~improve~~ SWR detection, we estimated the electrode ~~position~~ placements in the CA1 regions of the hippocampus using distinct multiunit

[1] Hippocampus: Distance = 1.11 [1.01], median [IQR], $n$ = 195,681 timepoints; EC: Distance = 0.94 [1.10], median [IQR], $n$ = 133,761 timepoints; Amygdala: Distance = 0.78 [0.88], median [IQR], $n$ = 165,281 timepoints.

[2] Hippocampus: Distance = 0.60 [0.70], median [IQR], $n$ = 8,772 combinations; EC: Distance = 0.28 [0.52], median [IQR], $n$ = 5,017 combinations ($p < 0.01$; Brunner–Munzel test); Amygdala: Distance = 0.24 [0.42], median [IQR], $n$ = 7,466 combinations ($p < 0.01$; Brunner–Munzel test).

[3] Correct rate: set size four (0.99 ±0.11, mean ±SD; $n$ = 333 trials) vs. set size six (0.93 ±0.26; $n$ = 278 trials; $p < 0.001$, Brunner–Munzel test with Bonferroni correction) and set size eight (0.87 ±0.34; $n$ = 275 trials; $p < 0.05$; Brunner–Munzel test with Bonferroni correction). Overall, $p < 0.001$ for Kruskal–Wallis test; correlation coefficient = -0.20, $p < 0.001$.

[4] Response time: set size four (1.26 ±0.45 s; $n$ = 333 trials) vs. set size six (1.53 ±0.91 s; $n$ = 278 trials) and set size eight (1.66 ±0.80 s; $n$ = 275 trials). All comparisons $p < 0.001$, Brunner–Munzel test with Bonferroni correction; $p < 0.001$ for Kruskal–Wallis test; correlation coefficient = 0.22, $p < 0.001$

[5] Correlation between set size and $\log_{10}(\|g_E g_R\|)$: correlation coefficient = 0.05, $p < 0.001$. Specific values: $\|g_E g_R\|$ = 0.54 [0.70] for set size four, $n$ = 447; $\|g_E g_R\|$ = 0.58 [0.66] for set size six, $n$ = 381; $\|g_E g_R\|$ = 0.61 [0.63] for set size eight, $n$ = 395.

spike patterns during the SWR events. ~~We embedded~~ $SWR^+/SWR^-$ candidates from ~~each~~ every session and hippocampal region were embedded in a two-dimensional space ~~via~~ using UMAP (Figure 4A).[6] ~~The quality of clustering was verified using~~ We used the silhouette score as a metric for quality of clustering (Figure 4B and Table 2). Recording sites ~~yielding~~ with an average silhouette score ~~over~~ exceeding 0.6 across all sessions were ~~designated~~ identified as putative CA1 regions.[7] (Tables 2 and 3). We ~~found~~ identified five putative CA1 regions, ~~out of which four weren't~~ four of which were not labeled as seizure onset zones (Table 1).

~~We further labeled~~ Subsequently, $SWR^+/SWR^-$ candidates within these putative CA1 regions were labeled as $SWR^+$ and $SWR^-$, respectively[8] (Table 3). Both $SWR^+$ and $SWR^-$ exhibited ~~equal duration~~the same duration[9] (Figure 4C) due to their definitions, and ~~adopted~~ followed a log-distribution. ~~There was an increase~~ We observed an augmentation in $SWR^+$ incidence ~~within the first~~ during the initial 400 ms of the retrieval phase[10] (Figure 4D). The peak ripple band amplitude of $SWR^+$ ~~was greater than that of~~ outpaced $SWR^-$ and followed a log-normal distribution (Figure 4E).[11].

### 2.5. *Transient changes in hippocampal neural ~~trajectories~~ trajectory during SWR~~events~~*

We ~~calculated~~ computed the distance of the trajectory from the origin ($O$) during SWR events in both the encoding and retrieval phases (Figure 5A). Observing ~~an~~ the increase in distance during SWR as shown in Figure 5A, we ~~classified~~ differentiated each SWR into three stages: pre-, mid-, and post-SWR. ~~Consequently~~Therefore, the distances from $O$ during ~~these SWR stages are denoted~~ those SWR periods are identified as $\|\text{pre-eSWR}^+\|$, $\|\text{mid-eSWR}^+\|$ among others.

~~The~~ $\|\text{mid-eSWR}^+\|$[12] was ~~larger~~ greater than $\|\text{pre-eSWR}^+\|$[13], and $\|\text{mid-rSWR}^+\|$[14] was ~~bigger~~ larger than $\|\text{pre-rSWR}^+\|$ in both Match IN and Mismatch OUT tasks.[15].

### 2.6. *Visualization of hippocampal neural ~~trajectories~~ trajectory during SWR in two-dimensional spaces*

Following our observations ~~on~~ of neural trajectory 'jumping' during ~~a SWR event~~ SWR (Figure 5), we visualized the three-dimensional trajectories of pre-, mid-, and post-SWR events during the encoding and retrieval phases (Figure 6), the distance between which was found to ~~depend on memory load~~ be memory-load dependent (Figure 3).

To ~~enable~~ provide two-dimensional visualization, we linearly aligned peri-SWR trajectories by assigning $g_E$ at the origin (0, 0) and $g_R$ at ($\|g_E g_R\|$, 0). ~~We then~~ Post this, we rotated these aligned trajectories around the $g_E g_R$ axis (the x-axis). ~~This method ensured that~~ Thus, the distances from the origin in the original three-dimensional spaces ~~were~~ are preserved in the two-dimensional ~~counterparts~~equivalent.

The scatter plot within these two-dimensional spaces ~~illustrate~~ reveals characteristic distributions of peri-SWR trajectories based on ~~the phases and types of task . One can observe , for example,~~ phases and task types. For instance, one can observe that the magnitude of $\|\text{mid-eSWR}^+\|$ surpasses that of $\|\text{pre-eSWR}^+\|$ (Figure 6B), ~~which is~~ consistent with our earlier findings (Figure 5).

### 2.7. *~~Directionality~~ Fluctuations of hippocampal neural trajectories between encoding and retrieval states*

~~We then investigated the~~ Next, we examined trajectory *directions* ~~of the trajectories~~ in relation to $\overrightarrow{g_E g_R}$. The directions of SWRs were defined by the neural trajectory at −250 ms and +250 ms from their center, ~~namely~~ i.e., $\overrightarrow{\text{eSWR}^+}$.

[6] Consider the AHL in session #1 of subject #1, for illustration purposes.

[7] The ~~designated~~ identified regions were: AHL of subject #1, AHR of subject #3, PHL of subject #4, AHL of subject #6, and AHR of subject #9.

[8] These definitions ~~resulted in~~ led to equal counts for both categories: $SWR^+$ ($n$ = 1,170) and $SWR^-$ ($n$ = 1,170).

[9] These definitions ~~resulted in~~ led to equal durations for both categories: $SWR^+$ (93.0 [65.4] ms) and $SWR^-$ (93.0 [65.4] ms).

[10] ~~The occurrence of~~ $SWR^+$ increased against the bootstrap sample; 95th percentile = 0.42 [Hz]; $p < 0.05$.

[11] $SWR^+$ (3.05 [0.85] SD of baseline, median [IQR]; $n$ = 1,170) vs. $SWR^-$ (2.37 [0.33] SD of baseline, median [IQR]; $n$ = 1,170; $p < 0.001$; Brunner–Munzel test).

[12] 1.25 [1.30], median [IQR], $n$ = 1,281, in Match IN task; 1.12 [1.35], median [IQR], $n$ = 1,163, in Mismatch OUT task

[13] 1.08 [1.07], median [IQR], $n$ = 1,149, in Match IN task; 0.90 [1.12], median [IQR], $n$ = 1,088, in Mismatch OUT task

[14] 1.32 [1.24], median [IQR], $n$ = 935, in Match IN task; 1.15 [1.26], median [IQR], $n$ = 891, in Mismatch OUT task

[15] 1.19 [0.96], median [IQR], $n$ = 673, in Match IN task; 0.94 [0.88], median [IQR], $n$ = 664, in Mismatch OUT task

We calculated the density of $\overrightarrow{\text{eSWR}} \cdot \overrightarrow{g_E g_R}$, $\overrightarrow{\text{rSWR}} \cdot \overrightarrow{g_E g_R}$, and $\overrightarrow{\text{eSWR}} \cdot \overrightarrow{\text{rSWR}}$ (Figures 7A–D). ~~The~~ $\overrightarrow{\text{rSWR}^-} \cdot \overrightarrow{g_E g_R}$ ~~demonstrated~~ displayed a biphasic distribution.

By ~~comparing~~ taking the difference between the distribution of $\overrightarrow{\text{rSWR}^+} \cdot \overrightarrow{g_E g_R}$ (Figures 7A and B) ~~with~~ and that of $\overrightarrow{\text{rSWR}^-} \cdot \overrightarrow{g_E g_R}$ (Figures 7C and D), we computed the contributions of SWR (Figures 7E and F), which ~~indicated~~ revealed a shift in the direction of $\overrightarrow{g_E g_R}$ (Figures 7E and F: *red rectangles*).

~~Furthermore, and only~~ Moreover, exclusively in the Mismatch OUT task, $\overrightarrow{\text{eSWR}^+} \cdot \overrightarrow{\text{rSWR}^+}$ was less than $\overrightarrow{\text{eSWR}^-} \cdot \overrightarrow{\text{rSWR}^-}$ (baseline periods) (Figure 7F: *pink circles*). ~~Put simply~~In simpler terms, eSWR and rSWR pointed in ~~opposite directions~~ the opposite direction only in the Mismatch OUT task but not in the Match IN task (Figure 7E: *pink circles*).

## 3. Discussion

## 4. Discussion

This study ~~posits that hippocampal neurons generate distinct trajectories~~ hypothesized that within low-dimensional spaces during a working memory (WM) task in humans, ~~specifically~~ hippocampal neurons form unique trajectories, particularly during sharp-wave ripple (SWR) periods. Initially, the multiunit spikes in ~~the~~ medial temporal lobe (MTL) regions were projected onto three-dimensional spaces during a Sternberg task using Gaussian Process Factor Analysis (GPFA) (Figure 1D–E and Figure 2A). The ~~trajectory distance~~ distance of the trajectory across WM phases ($\|g_F g_E\|$, $\|g_F g_M\|$, $\|g_F g_R\|$, $\|g_E g_M\|$, $\|g_E g_R\|$, and $\|g_M g_R\|$) was ~~markedly~~ notably larger in the hippocampus than in the EC and amygdala (Figure 2E), ~~which implies~~ indicating dynamic neural activity in the hippocampus during the WM task. ~~Additionally~~Further, in the hippocampus, the trajectory distance between the encoding and retrieval phases ($\|g_F g_E\|$) ~~was found to positively correlate~~ exhibited a positive correlation with memory load (Figure 3C–D), ~~denoting~~ reflecting WM processing. The hippocampal neural trajectory ~~momentarily increased~~ was found to increase transiently during SWRs (Figure 5). ~~Eventually~~Finally, the hippocampal neural trajectory ~~alternated~~ switched between encoding and retrieval states, ~~progressing specifically~~ moving from encoding to retrieval during SWR events (Figure 7). ~~Such discoveries not only interpret varying aspects~~ These findings not only explain various facets of hippocampal neural activity during a WM task in humans ~~,~~ but also offer ~~fresh~~ new insights into how SWRs ~~help alter~~ influence the switch in neural states.

~~Our findings show~~ We found that the distance of ~~hippocampal~~ the neural trajectory across the phases ~~, even after~~ was greater in the hippocampus compared to that in the EC and amygdala, even when considering the distance from $O$ in these regions ~~, surpassed that in the EC and amygdala~~ (Figure 2C–E). This ~~reaffirms the participation~~ supports the involvement of the hippocampus in the WM task, ~~coinciding with prior assertions~~ aligning with previous reports of hippocampal persistent firing during the maintenance phase [3] [4] [5] [6]. However, when ~~applying~~ we applied GPFA to multiunit activity during a 1-second level resolution of the WM task, we ~~noticed~~ observed that the neural trajectory in low-dimensional space ~~demonstrated~~ showed a memory-load ~~dependence between~~ dependency between the encoding and retrieval phases, ~~denoted~~ symbolized as $\|g_E g_R\|$ (Figure 3). ~~This supports the association between the hippocampus and~~ These findings corroborate the association of the hippocampus with WM processing.

Our analysis ~~focused on~~ was confined to putative CA1 regions (Figure 4), which ~~is supported by various contributions~~was bolstered by several factors. This specific ~~concentration arises from well-established observations where SWRs coincide with spike clusters~~ focus stems from established observations that SWRs synchronize with spike bursts of interneurons and pyramidal neurons [44] [45] [46] [47], potentially within a 50 $\mu$m radius of the recording site [48]. ~~An increase in the instances of SWRs was identified~~ We further identified an increased incidence of SWRs during the first 0–400 ms of the retrieval phase (Figure 4D). This ~~observation aligns with earlier reports of increased SWR occurrence before~~ finding harmonizes with previous reports of heightened SWR occurrence preceding spontaneous verbal recall [21] [22], ~~reinforcing our findings~~ supporting our results under a triggered retrieval condition. The observed log-normal distributions of both SWR ~~length~~ duration and ripple band peak amplitude ~~observed~~ in this study (Figure 4C & E) ~~concur with the field's consensus [39]. Consequently, confining recordings~~

is in accordance with the consensus in this field [39] . As a result, our decision to restrict recording sites to putative CA1 regions likely ~~improved~~ contributed to enhancing the accuracy of SWR detection. However, the ~~observed~~ increase in trajectory distance from $O$ during SWRs (Figure 5) ~~may be skewed higher~~ might have been skewed towards higher values due to channel selection. ~~Nevertheless~~However, this potential bias does not ~~significantly undermine our primary conclusions~~substantially challenge our primary findings.

Interestingly, during the retrieval phase, ~~trajectory directions alternated~~ the trajectory directions oscillated between encoding and retrieval states ~~both during~~ during both baseline and SWR periods (Figure 7C & D). ~~Furthermore~~Moreover, the balance of this oscillation ~~transitioned~~ shifted from encoding to retrieval state during SWR ~~episodes~~ events (Figure 7 E & F). These ~~outcomes align with preceding reports regarding~~ results are consistent with previous reports on the role of ~~SWRs~~ SWR in memory retrieval [21] [22]. Our findings ~~suggest a novel understandingwhere~~ highlight a new understanding, suggesting that SWRs occur when the hippocampal representation transitions from encoding to retrieval states~~, thereby revealing unexplored~~. Therefore, these results reveal novel aspects of hippocampal representations, ~~such as~~ including (i) neuronal oscillation between encoding and retrieval ~~phases~~ states during a WM task ~~,~~ and (ii) SWR ~~functioning as a catalyst~~ serving as a trigger for changing neural states.

~~Moreover~~Furthermore, our study ~~identified~~ uncovered WM-task type-specific differences between encoding- and retrieval-SWRs (Figure 7E–F)~~specific to WM-task types~~. Notably, ~~counter~~ opposing movements of encoding-SWR (eSWR) and retrieval-SWR (rSWR) were not ~~seen~~ observed in the Match IN task but were ~~evident~~ apparent in the Mismatch OUT task. ~~The~~ These observations can be explained by the memory engram theory ~~can explain these observations [49]. The~~ [49]. Particularly, the Match In task ~~, for instance, presented participants with previous letters, whereas~~ provided participants with previously presented letters, contrastingly, the Mismatch OUT task introduced a new letter ~~absent~~ not present in the encoding phase. These interpretations ~~highlight the vital~~ underscore the significant role of SWR in human cognitive processes.

In conclusion, ~~this~~ the present investigation demonstrated that ~~during a WM task,~~ hippocampal activity oscillates between encoding and retrieval states ~~,~~ ~~uniquely transitioning~~ during a WM task and uniquely transitions from encoding to retrieval during SWR ~~events~~incidents. These findings ~~offer valuable insights~~ provide meaningful insight into the neural ~~substrates and workings~~ counterparts and functionality of working memory ~~within~~ in the hippocampus.

## References


[1] W. B. Scoville, B. Milner, LOSS OF RECENT MEMORY AFTER BILATERAL HIPPOCAMPAL LESIONS, Journal of Neurology, Neurosurgery, and Psychiatry 20 (1) (1957) 11–21. URL https://www.ncbi.nlm.nih.gov/pmc/articles/PMC497229/

[2] L. R. Squire, The Legacy of Patient H.M. for Neuroscience, Neuron 61 (1) (2009) 6–9. doi:10.1016/j.neuron.2008.12.023.
URL https://www.ncbi.nlm.nih.gov/pmc/articles/PMC2649674/

[3] E. Boran, T. Fedele, P. Klaver, P. Hilfiker, L. Stieglitz, T. Grunwald, J. Sarnthein, Persistent hippocampal neural firing and hippocampal-cortical coupling predict verbal working memory load, Science Advances 5 (3) (2019) eaav3687. doi:10.1126/sciadv.aav3687.
URL https://www.science.org/doi/10.1126/sciadv.aav3687

[4] J. Kamiński, S. Sullivan, J. M. Chung, I. B. Ross, A. N. Mamelak, U. Rutishauser, Persistently active neurons in human medial frontal and medial temporal lobe support working memory, Nature Neuroscience 20 (4) (2017) 590–601, number: 4 Publisher: Nature Publishing Group. doi:10.1038/nn.4509.
URL https://www.nature.com/articles/nn.4509

[5] S. Kornblith, R. Q. Quiroga, C. Koch, I. Fried, F. Mormann, Persistent Single-Neuron Activity during Working Memory in the Human Medial Temporal Lobe, Current Biology 27 (7) (2017) 1026–1032, publisher: Elsevier. doi:10.1016/j.cub.2017.02.013.
URL https://www.cell.com/current-biology/abstract/S0960-9822(17)30149-5

[6] M. C. M. Faraut, A. A. Carlson, S. Sullivan, O. Tudusciuc, I. Ross, C. M. Reed, J. M. Chung, A. N. Mamelak, U. Rutishauser, Dataset of human medial temporal lobe single neuron activity during declarative memory encoding and recognition, Scientific Data 5 (1) (2018) 180010, number: 1 Publisher: Nature Publishing Group. doi:10.1038/sdata.2018.10.
URL https://www.nature.com/articles/sdata201810

[7] A. A. Borders, C. Ranganath, A. P. Yonelinas, The hippocampus supports high-precision binding in visual working memory, Hippocampus 32 (3) (2022) 217–230. doi:10.1002/hipo.23401.

[8] J. Li, D. Cao, S. Yu, X. Xiao, L. Imbach, L. Stieglitz, J. Sarnthein, T. Jiang, Functional specialization and interaction in the amygdala-hippocampus circuit during working memory processing, Nature Communications 14 (1) (2023)

2921, number: 1 Publisher: Nature Publishing Group. doi:10.1038/s41467-023-38571-w.
URL https://www.nature.com/articles/s41467-023-38571-w

[9] V. Dimakopoulos, P. Mégevand, L. H. Stieglitz, L. Imbach, J. Sarnthein, Information flows from hippocampus to auditory cortex during replay of verbal working memory items, eLife 11 (2022) e78677, publisher: eLife Sciences Publications, Ltd. doi:10.7554/eLife.78677.
URL https://doi.org/10.7554/eLife.78677

[10] G. Buzsáki, Hippocampal sharp wave-ripple: A cognitive biomarker for episodic memory and planning, Hippocampus 25 (10) (2015) 1073–1188, _eprint: https://onlinelibrary.wiley.com/doi/pdf/10.1002/hipo.22488. doi:https://doi.org/10.1002/hipo.22488.
URL https://onlinelibrary.wiley.com/doi/abs/10.1002/hipo.22488

[11] M. A. Wilson, B. L. McNaughton, Reactivation of hippocampal ensemble memories during sleep, Science (New York, N.Y.) 265 (5172) (1994) 676–679. doi:10.1126/science.8036517.

[12] Z. Nádasdy, H. Hirase, A. Czurkó, J. Csicsvari, G. Buzsáki, Replay and Time Compression of Recurring Spike Sequences in the Hippocampus, Journal of Neuroscience 19 (21) (1999) 9497–9507, publisher: Society for Neuroscience Section: ARTICLE. doi:10.1523/JNEUROSCI.19-21-09497.1999.
URL https://www.jneurosci.org/content/19/21/9497

[13] A. K. Lee, M. A. Wilson, Memory of sequential experience in the hippocampus during slow wave sleep, Neuron 36 (6) (2002) 1183–1194. doi:10.1016/s0896-6273(02)01096-6.

[14] K. Diba, G. Buzsáki, Forward and reverse hippocampal place-cell sequences during ripples, Nature Neuroscience 10 (10) (2007) 1241–1242, number: 10 Publisher: Nature Publishing Group. doi:10.1038/nn1961.
URL https://www.nature.com/articles/nn1961

[15] T. J. Davidson, F. Kloosterman, M. A. Wilson, Hippocampal replay of extended experience, Neuron 63 (4) (2009) 497–507. doi:10.1016/j.neuron.2009.07.027.

[16] G. Girardeau, K. Benchenane, S. I. Wiener, G. Buzsáki, M. B. Zugaro, Selective suppression of hippocampal ripples impairs spatial memory, Nature Neuroscience 12 (10) (2009) 1222–1223. doi:10.1038/nn.2384.
URL http://www.nature.com/articles/nn.2384

[17] V. Ego-Stengel, M. A. Wilson, Disruption of ripple-associated hippocampal activity during rest impairs spatial learning in the rat, Hippocampus 20 (1) (2010) 1–10. doi:10.1002/hipo.20707.

[18] A. Fernández-Ruiz, A. Oliva, E. Fermino de Oliveira, F. Rocha-Almeida, D. Tingley, G. Buzsáki, Long-duration hippocampal sharp wave ripples improve memory, Science (New York, N.Y.) 364 (6445) (2019) 1082–1086. doi:10.1126/science.aax0758.
URL https://www.ncbi.nlm.nih.gov/pmc/articles/PMC6693581/

[19] J. Kim, A. Joshi, L. Frank, K. Ganguly, Cortical–hippocampal coupling during manifold exploration in motor cortex, Nature (2022) 1–8Publisher: Nature Publishing Group. doi:10.1038/s41586-022-05533-z.
URL https://www.nature.com/articles/s41586-022-05533-z

[20] C.-T. Wu, D. Haggerty, C. Kemere, D. Ji, Hippocampal awake replay in fear memory retrieval, Nature Neuroscience 20 (4) (2017) 571–580. doi:10.1038/nn.4507.

[21] Y. Norman, E. M. Yeagle, S. Khuvis, M. Harel, A. D. Mehta, R. Malach, Hippocampal sharp-wave ripples linked to visual episodic recollection in humans, Science 365 (6454) (2019) eaax1030. doi:10.1126/science.aax1030.
URL https://www.sciencemag.org/lookup/doi/10.1126/science.aax1030

[22] Y. Norman, O. Raccah, S. Liu, J. Parvizi, R. Malach, Hippocampal ripples and their coordinated dialogue with the default mode network during recent and remote recollection, Neuron 109 (17) (2021) 2767–2780.e5, publisher: Elsevier. doi:10.1016/j.neuron.2021.06.020.
URL https://www.cell.com/neuron/abstract/S0896-6273(21)00461-X

[23] C. J. Behrens, L. P. van den Boom, L. de Hoz, A. Friedman, U. Heinemann, Induction of sharp wave–ripple complexes in vitro and reorganization of hippocampal networks, Nature Neuroscience 8 (11) (2005) 1560–1567, number: 11 Publisher: Nature Publishing Group. doi:10.1038/nn1571.
URL https://www.nature.com/articles/nn1571

[24] H. Norimoto, K. Makino, M. Gao, Y. Shikano, K. Okamoto, T. Ishikawa, T. Sasaki, H. Hioki, S. Fujisawa, Y. Ikegaya, Hippocampal ripples down-regulate synapses, Science (New York, N.Y.) 359 (6383) (2018) 1524–1527. doi:10.1126/science.aao0702.

[25] S. P. Jadhav, C. Kemere, P. W. German, L. M. Frank, Awake Hippocampal Sharp-Wave Ripples Support Spatial Memory, Science 336 (6087) (2012) 1454–1458, publisher: American Association for the Advancement of Science. doi:10.1126/science.1217230.
URL https://www.science.org/doi/abs/10.1126/science.1217230

[26] J. O'Keefe, J. Dostrovsky, The hippocampus as a spatial map: Preliminary evidence from unit activity in the freely-moving rat, Brain Research 34 (1971) 171–175, place: Netherlands Publisher: Elsevier Science. doi:10.1016/0006-8993(71)90358-1.

[27] J. O'Keefe, Place units in the hippocampus of the freely moving rat, Experimental Neurology 51 (1) (1976) 78–109. doi:10.1016/0014-4886(76)90055-8.
URL https://www.sciencedirect.com/science/article/pii/0014488676900558

[28] A. D. Ekstrom, M. J. Kahana, J. B. Caplan, T. A. Fields, E. A. Isham, E. L. Newman, I. Fried, Cellular networks underlying human spatial navigation, Nature 425 (6954) (2003) 184–188, number: 6954 Publisher: Nature Publishing Group. doi:10.1038/nature01964.
URL https://www.nature.com/articles/nature01964

[29] K. B. Kjelstrup, T. Solstad, V. H. Brun, T. Hafting, S. Leutgeb, M. P. Witter, E. I. Moser, M.-B. Moser, Finite Scale of Spatial Representation in the Hippocampus, Science 321 (5885) (2008) 140–143, publisher: American Association for the Advancement of Science. doi:10.1126/science.1157086.
URL https://www.science.org/doi/abs/10.1126/science.1157086

[30] C. D. Harvey, F. Collman, D. A. Dombeck, D. W. Tank, Intracellular dynamics of hippocampal place cells during virtual navigation, Nature 461 (7266) (2009) 941–946, number: 7266 Publisher: Nature Publishing Group. doi:10.1038/nature08499.
URL https://www.nature.com/articles/nature08499

[31] H. Zhang, P. D. Rich, A. K. Lee, T. O. Sharpee, Hippocampal spatial representations exhibit a hyperbolic geometry that expands with experience, Nature Neuroscience (Dec. 2022). doi:10.1038/s41593-022-01212-4.
URL https://www.nature.com/articles/s41593-022-01212-4

[32] P. A. Naber, F. H. Lopes da Silva, M. P. Witter, Reciprocal connections between the entorhinal cortex and hippocampal fields CA1 and the subiculum are in register with the projections from CA1 to the subiculum, Hippocampus 11 (2) (2001) 99–104, _eprint: https://onlinelibrary.wiley.com/doi/pdf/10.1002/hipo.1028. doi:10.1002/hipo.1028.
URL https://onlinelibrary.wiley.com/doi/abs/10.1002/hipo.1028

[33] N. M. van Strien, N. L. M. Cappaert, M. P. Witter, The anatomy of memory: an interactive overview of the parahippocampal–hippocampal network, Nature Reviews Neuroscience 10 (4) (2009) 272–282, number: 4 Publisher: Nature Publishing Group. doi:10.1038/nrn2614.
URL https://www.nature.com/articles/nrn2614

[34] B. A. Strange, M. P. Witter, E. S. Lein, E. I. Moser, Functional organization of the hippocampal longitudinal axis, Nature Reviews Neuroscience 15 (10) (2014) 655–669, number: 10 Publisher: Nature Publishing Group. doi:10.1038/nrn3785.
URL https://www.nature.com/articles/nrn3785

[35] R. J. Gardner, E. Hermansen, M. Pachitariu, Y. Burak, N. A. Baas, B. A. Dunn, M.-B. Moser, E. I. Moser, Toroidal topology of population activity in grid cells, Nature 602 (7895) (2022) 123–128, number: 7895 Publisher: Nature Publishing Group. doi:10.1038/s41586-021-04268-7.
URL https://www.nature.com/articles/s41586-021-04268-7

[36] E. Boran, T. Fedele, A. Steiner, P. Hilfiker, L. Stieglitz, T. Grunwald, J. Sarnthein, Dataset of human medial temporal lobe neurons, scalp and intracranial EEG during a verbal working memory task, Scientific Data 7 (1) (2020) 30, number: 1 Publisher: Nature Publishing Group. doi:10.1038/s41597-020-0364-3.
URL https://www.nature.com/articles/s41597-020-0364-3

[37] B. M. Yu, J. P. Cunningham, G. Santhanam, S. I. Ryu, K. V. Shenoy, M. Sahani, Gaussian-Process Factor Analysis for Low-Dimensional Single-Trial Analysis of Neural Population Activity, Journal of Neurophysiology 102 (1) (2009) 614–635. doi:10.1152/jn.90941.2008.
URL https://www.ncbi.nlm.nih.gov/pmc/articles/PMC2712272/

[38] J. Niediek, J. Boström, C. E. Elger, F. Mormann, Reliable Analysis of Single-Unit Recordings from the Human Brain under Noisy Conditions: Tracking Neurons over Hours, PLOS ONE 11 (12) (2016) e0166598, publisher: Public Library of Science. doi:10.1371/journal.pone.0166598.
URL https://journals.plos.org/plosone/article?id=10.1371/journal.pone.0166598

[39] A. A. Liu, S. Henin, S. Abbaspoor, A. Bragin, E. A. Buffalo, J. S. Farrell, D. J. Foster, L. M. Frank, T. Gedankien, J. Gotman, J. A. Guidera, K. L. Hoffman, J. Jacobs, M. J. Kahana, L. Li, Z. Liao, J. J. Lin, A. Losonczy, R. Malach, M. A. van der Meer, K. McClain, B. L. McNaughton, Y. Norman, A. Navas-Olive, L. M. de la Prida, J. W. Rueckemann, J. J. Sakon, I. Skelin, I. Soltesz, B. P. Staresina, S. A. Weiss, M. A. Wilson, K. A. Zaghloul, M. Zugaro, G. Buzsáki, A consensus statement on detection of hippocampal sharp wave ripples and differentiation from other fast oscillations, Nature Communications 13 (1) (2022) 6000, number: 1 Publisher: Nature Publishing Group. doi:10.1038/s41467-022-33536-x.
URL https://www.nature.com/articles/s41467-022-33536-x

[40] K. Kay, M. Sosa, J. E. Chung, M. P. Karlsson, M. C. Larkin, L. M. Frank, A hippocampal network for spatial coding during immobility and sleep, Nature 531 (7593) (2016) 185–190. doi:10.1038/nature17144.

[41] L. McInnes, J. Healy, N. Saul, L. Großberger, UMAP: Uniform Manifold Approximation and Projection, Journal of Open Source Software 3 (29) (2018) 861. doi:10.21105/joss.00861.
URL https://joss.theoj.org/papers/10.21105/joss.00861

[42] P. J. Rousseeuw, Silhouettes: A graphical aid to the interpretation and validation of cluster analysis, Journal of Computational and Applied Mathematics 20 (1987) 53–65. doi:10.1016/0377-0427(87)90125-7.
URL https://www.sciencedirect.com/science/article/pii/0377042787901257

[43] P. Virtanen, R. Gommers, T. E. Oliphant, M. Haberland, T. Reddy, D. Cournapeau, E. Burovski, P. Peterson, W. Weckesser, J. Bright, S. J. van der Walt, M. Brett, J. Wilson, K. J. Millman, N. Mayorov, A. R. J. Nelson, E. Jones, R. Kern, E. Larson, C. J. Carey, Polat, Y. Feng, E. W. Moore, J. VanderPlas, D. Laxalde, J. Perktold, R. Cimrman, I. Henriksen, E. A. Quintero, C. R. Harris, A. M. Archibald, A. H. Ribeiro, F. Pedregosa, P. van Mulbregt, SciPy 1. 0 Contributors, SciPy 1.0: fundamental algorithms for scientific computing in Python, Nature Methods 17 (2020) 261–272, aDS Bibcode: 2020NatMe..17..261V. doi:10.1038/s41592-019-0686-2.
URL https://ui.adsabs.harvard.edu/abs/2020NatMe..17..261V

[44] G. Buzsáki, Two-stage model of memory trace formation: a role for "noisy" brain states, Neuroscience 31 (3) (1989) 551–570. doi:10.1016/0306-4522(89)90423-5.

[45] M. L. V. Quyen, A. Bragin, R. Staba, B. Crépon, C. L. Wilson, J. Engel, Cell Type-Specific Firing during Ripple Oscillations in the Hippocampal Formation of Humans, Journal of Neuroscience 28 (24) (2008) 6104–6110, publisher: Society for Neuroscience Section: Brief Communications. doi:10.1523/JNEUROSCI.0437-08.2008.
URL https://www.jneurosci.org/content/28/24/6104

[46] S. Royer, B. V. Zemelman, A. Losonczy, J. Kim, F. Chance, J. C. Magee, G. Buzsáki, Control of timing, rate and bursts of hippocampal place cells by dendritic and somatic inhibition, Na-

ture Neuroscience 15 (5) (2012) 769–775, number: 5 Publisher: Nature Publishing Group. doi:10.1038/nn.3077.
URL https://www.nature.com/articles/nn.3077

[47] N. Hájos, M. R. Karlócai, B. Németh, I. Ulbert, H. Monyer, G. Szabó, F. Erdélyi, T. F. Freund, A. I. Gulyás, Input-output features of anatomically identified CA3 neurons during hippocampal sharp wave/ripple oscillation in vitro, The Journal of Neuroscience: The Official Journal of the Society for Neuroscience 33 (28) (2013) 11677–11691. doi:10.1523/JNEUROSCI.5729-12.2013.

[48] E. W. Schomburg, C. A. Anastassiou, G. Buzsáki, C. Koch, The Spiking Component of Oscillatory Extracellular Potentials in the Rat Hippocampus, The Journal of Neuroscience 32 (34) (2012) 11798–11811. doi:10.1523/JNEUROSCI.0656-12.2012.
URL https://www.ncbi.nlm.nih.gov/pmc/articles/PMC3459239/

[49] X. Liu, S. Ramirez, P. T. Pang, C. B. Puryear, A. Govindarajan, K. Deisseroth, S. Tonegawa, Optogenetic stimulation of a hippocampal engram activates fear memory recall, Nature 484 (7394) (2012) 381–385, number: 7394 Publisher: Nature Publishing Group. doi:10.1038/nature11028.
URL https://www.nature.com/articles/nature11028

## Contributors

Y.W. and T.Y. conceptualized the study; Y.W. performed the data analysis; Y.W. and T.Y. wrote the original draft; and all authors reviewed the final manuscript.

## Acknowledgments

This research was funded by a grant from the Exploratory Research for Advanced Technology (JPMJER1801).

## Declaration of Interests

The authors declare that they have no competing interests.

## Data and code availability

The data is available on G-Node (https://doi.gin.g-node.org/10.12751/g-node.d76994/).
The source code is available on GitHub (https://github.com/yanagisawa-lab/hippocampal-neural-fluctuation-during-a-WM-task-in-humans).

## Inclusion and Diversity Statement

We support inclusive, diverse, and equitable conduct of research.

## Declaration of Generative AI in Scientific Writing

The authors employed ChatGPT, provided by OpenAI, for enhancing the manuscript's English language quality. After incorporating the suggested improvements, the authors meticulously revised the content. Ultimate responsibility for the final content of this publication rests entirely with the authors.

**Tables**

| Subject ID | of sessions | AHL | AHR | PHL | PHR | ECL | ECR | AL | AR | SOZ |
|---|---|---|---|---|---|---|---|---|---|---|
| 1 | 4 | o | x | o | o | o | x | o | x | "AHR, LR" |
| 2 | 7 | o | o | o | o | o | o | o | o | "AHR, PHR" |
| 3 | 3 | o | o | o | o | o | o | o | x | "AHL, PHL" |
| 4 | 2 | o | o | o | o | o | o | o | o | "AHL, AHR, PHL, PHR" |
| 5 | 3 | o | x | x | o | x | x | o | x | DRR |
| 6 | 6 | o | o | o | o | o | o | o | o | "AHL, PHL, ECL, AL" |
| 7 | 4 | o | o | o | o | o | o | o | o | "AHR, PHR" |
| 8 | 5 | o | o | o | o | o | o | o | o | ECR |
| 9 | 2 | o | o | o | o | o | o | o | o | "ECR, AR" |

**Table 1 – ~~Electrode Distribution within the Dataset~~ Distribution of Electrodes within the Dataset**

~~The~~ This figure ~~outlines~~ represents the electrode placements and the seizure onset zones. ~~Areas labelled~~ Regions designated with "o" ~~are included~~ were available in the dataset, ~~while~~ whereas those ~~indicated by~~ marked with "x" (*navy*) ~~are absent~~were not present. ~~Denoted abbreviations~~Abbreviations include: AHL, left hippocampal head; AHR, right hippocampal head; PHL, left hippocampal body; PHR, right hippocampal body; ECL, left entorhinal cortex; ECR, right entorhinal cortex; AL, left amygdala; AR, right amygdala~~.~~; and SOZ ~~refers to~~ symbolizes the seizure onset zone.

| Subject | AHL | AHR | PHL | PHR |
|---|---|---|---|---|
| 1 | 0.60 ± 0.14 | n.a. | n.a. | 0.1 ± 0 |
| 2 | 0.21 ± 0.16 | 0.17 ± 0.21 | 0.18 ± 0.22 | 0.20 ± 0.15 |
| 3 | 0.40 ± 0.42 | 0.83 ± 0.12 | n.a. | n.a. |
| 4 | 0.10 ± 0.00 | 0.10 ± 0.00 | 0.90 ± 0.00 | 0.10 ± 0.14 |
| 5 | n.a. | n.a. | n.a. | n.a. |
| 6 | 0.63 ± 0.06 | n.a. | n.a. | 0.27 ± 0.06 |
| 7 | 0.10 ± 0.00 | 0.35 ± 0.35 | 0.37 ± 0.47 | 0.10 ± 0.00 |
| 8 | 0.13 ± 0.10 | n.a. | 0.28 ± 0.49 | n.a. |
| 9 | n.a. | 0.85 ± 0.07 | 0.15 ± 0.07 | n.a. |

**Table 2** – ~~**Silhouette scores of UMAP clustering for $SWR^+$ candidates and $SWR^-$ candidates**~~ **Silhouette score of UMAP clustering for $SWR^+$ candidates and $SWR^-$ candidates**

The silhouette scores (mean ± SD across sessions per subject) ~~pertaining to~~ for UMAP clustering of SWR+ candidates and SWR candidates ~~are calculated and presented in~~ (Figure 4A~~. These calculations are~~ ) were calculated based on their corresponding multiunit spike patterns ~~, where the~~ (mean values ~~observed are~~ were 0.205 ~~with a standard deviation of~~ [0.285~~. The~~ ], median ~~and interquartile range are also presented (see~~ [IQR]; Figure 4B).

| Subject ID | of sessions | of trials | ROI | of SWRs | SWR incidence [Hz] |
|---|---|---|---|---|---|
| 1 | 2 | 100 | AHL | 274 | 0.34 |
| 3 | 2 | 97 | AHR | 325 | 0.42 |
| 4 | 2 | 99 | PHL | 202 | 0.26 |
| 6 | 2 | 100 | AHL | 297 | 0.37 |
| 9 | 2 | 97 | AHR | 72 | 0.09 |
| Total = 10 | Total = 493 | "Total = 1,170" | 0.30 ± 0.13 (mean ± SD) | | |

**Table 3** – ~~**Accounting for Specific SWR Events**~~ **Accounting for Defined SWR Events**

The table ~~compiles~~ collates statistics ~~related to assumed~~ of putative CA1 regions and SWR events. ~~To minimize sampling bias, only~~ Only the ~~initial~~ first two sessions (sessions 1 and 2) from each subject were ~~utilized~~considered to minimize sampling bias.

**Figures**

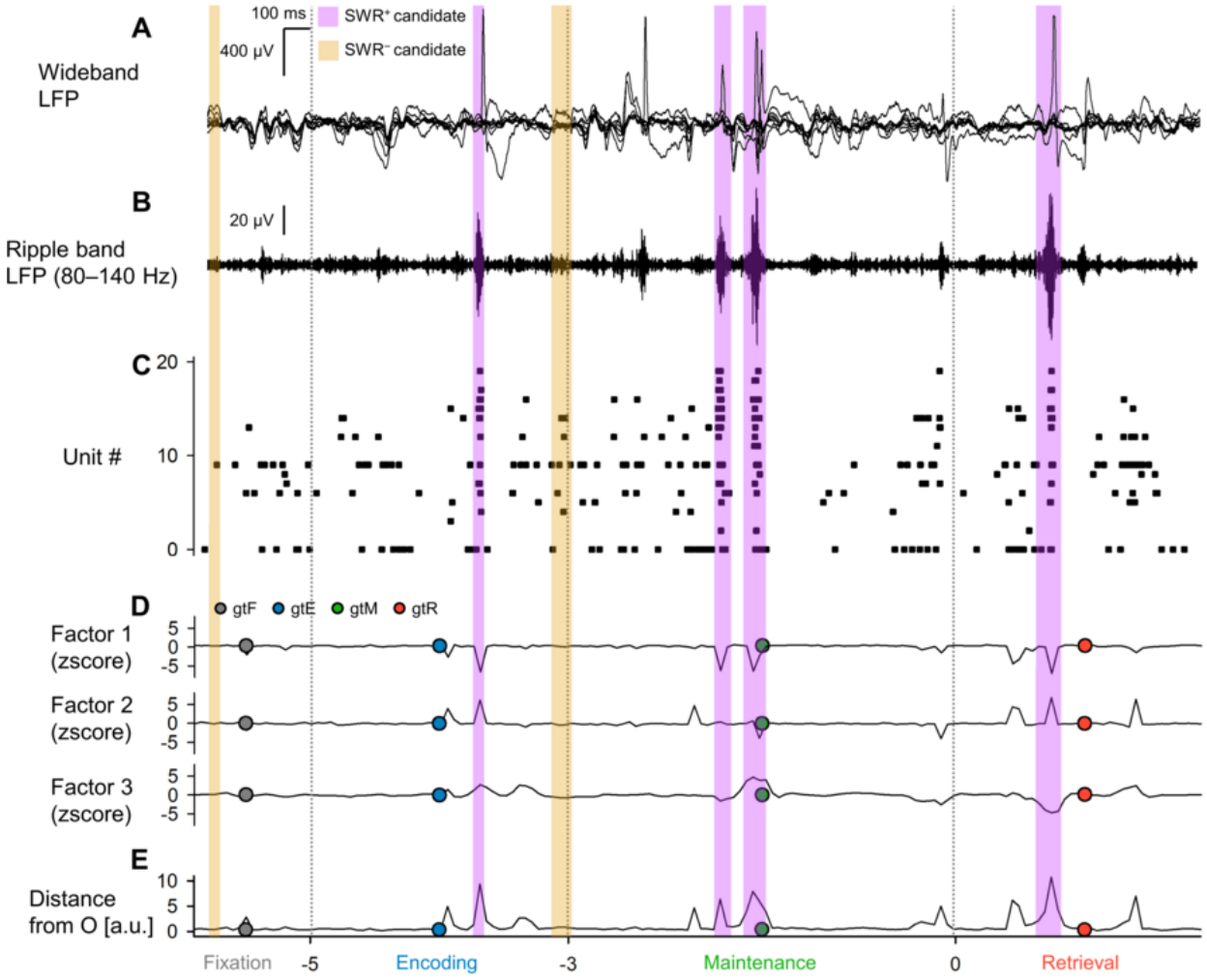


**Figure 1 – Local Field Potentials (LFP), Multiunit Activity, and Neural Trajectories in the Hippocampus During a Modified Sternberg Task**

***A.*** These traces show representative wideband LFP intracranial EEG (iEEG) signals recorded from the left hippocampal head. The subject performed a modified Sternberg working memory task, which includes fixation (1 s, *gray*), encoding (2 s, *blue*), maintenance (3 s, *green*), and retrieval (2 s, *red*). ***B.*** We then present the corresponding ripple band LFP traces. ***C.*** The raster plot depicts multiunit spikes taken from the LFP traces, sorted using a spike algorithm [38]. ***D.*** Subsequently, we illustrate the neural trajectories, which are calculated by GPFA on spike counts per unit with 50-ms bins. Each phase's geometric median is marked by the dot circles. ***E.*** The trajectory's distance from the origin $O$ is portrayed, with *purple* and *yellow* rectangles indicating the timings for $SWR^+$ candidates and $SWR^-$ candidates (considered as controls for $SWR^+$), respectively.

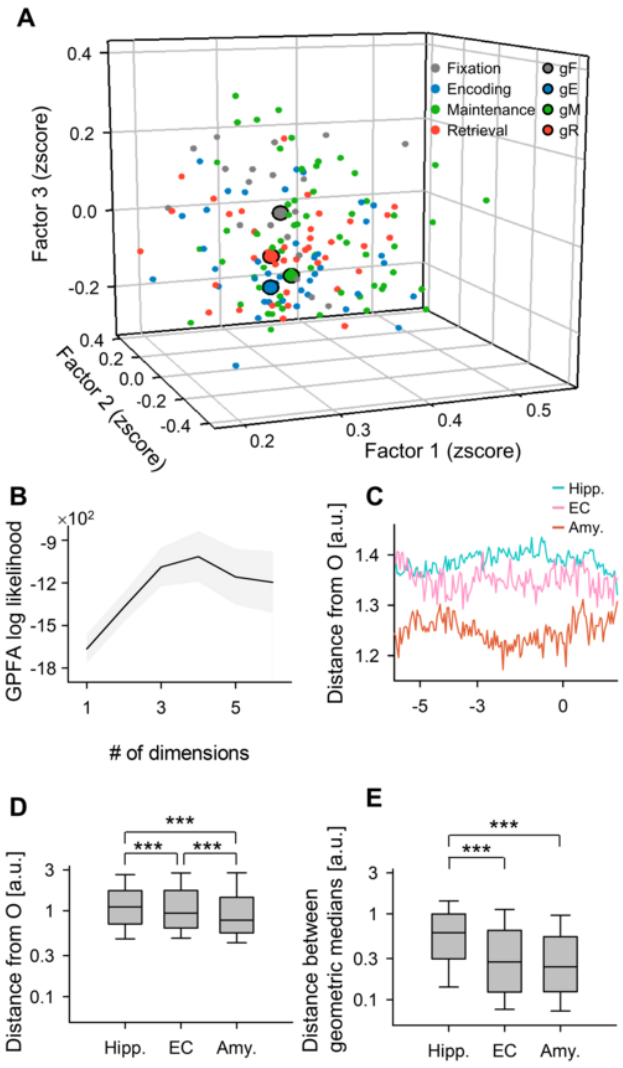


**Figure 2 – State-Dependent Trajectories of Hippocampal Neurons**

***A.*** Neural trajectories within the initial three-dimensional factors derived from the Gaussian Process Factor Analysis (GPFA) are displayed. The smaller dots correspond to coordinates of 50-ms neural trajectory bins, while the larger dots with *black* edges signify the geometric medians for respective stages in the Sternberg working memory task: fixation (*gray*), encoding (*blue*), maintenance (*green*), and retrieval (*red*). ***B.*** The figure conveys the log-likelihood of the GPFA models versus the count of dimensions used to embed multiunit spikes found in the medial temporal lobe (MTL) territories. In specific, the elbow method pinpointed the optimal dimension to be three. ***C.*** This panel illustrates the distance of the neural trajectories from the origin (*O*) for the hippocampus (Hipp.), entorhinal cortex (EC), and amygdala (Amy.), against the time elapsed from the probe onset. ***D.*** The distance of the trajectory from *O* within MTL regions is displayed. The hippocampus shows the farthest distance, followed by the EC and the Amygdala. ***E.*** The plot represents inter-phase trajectory distances within the MTL regions. Abbreviations:

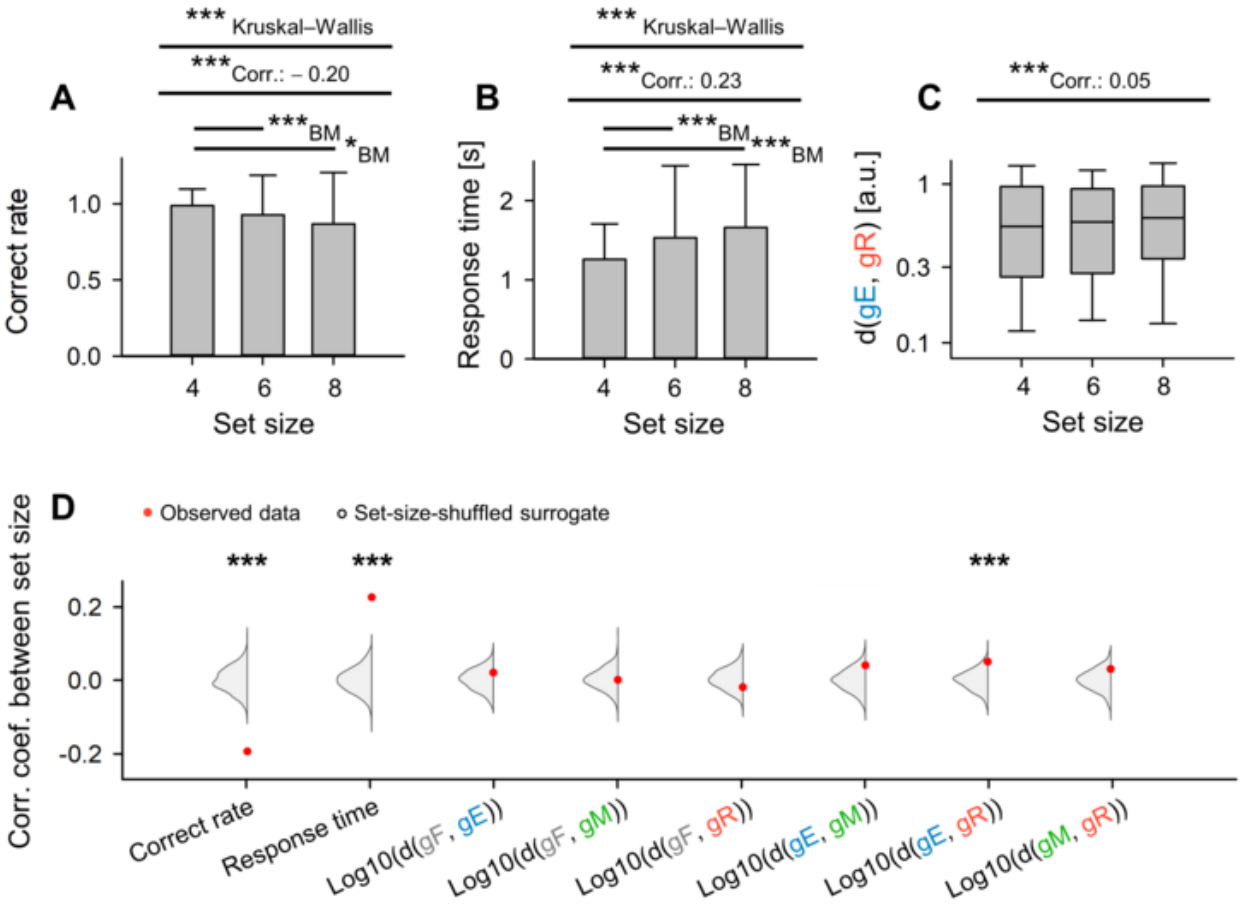


**Figure 3 – Dependency of Trajectory Distance on Memory Load: Encoding and Retrieval States in Hippocampus**

***A.*** The relationship between set size (number of letters that need to be encoded) and correct rate in the working memory task (coefficient = −0.20, ***$p < 0.001$). ***B.*** The correlation between set size and response time (coefficient = 0.23, ***$p < 0.001$). ***C.*** The impact of set size on the inter-phase distances between the encoding and retrieval phases ($\|g_E g_R\|$) (correlation coefficient = 0.05). ***D.*** *Red* dots represent experimental observations of correlations between set size and the following parameters: correct rate, response time, $\log_{10}\|g_F g_E\|$, $\log_{10}\|g_F g_M\|$, $\log_{10}\|g_F g_R\|$, $\log_{10}\|g_E g_M\|$, $\log_{10}\|g_E g_R\|$, and $\log_{10}\|g_M g_R\|$. The *gray* kernel density plot illustrates the corresponding set-size-shuffled surrogate ($n$ = 1,000) (***$p$s < 0.001).

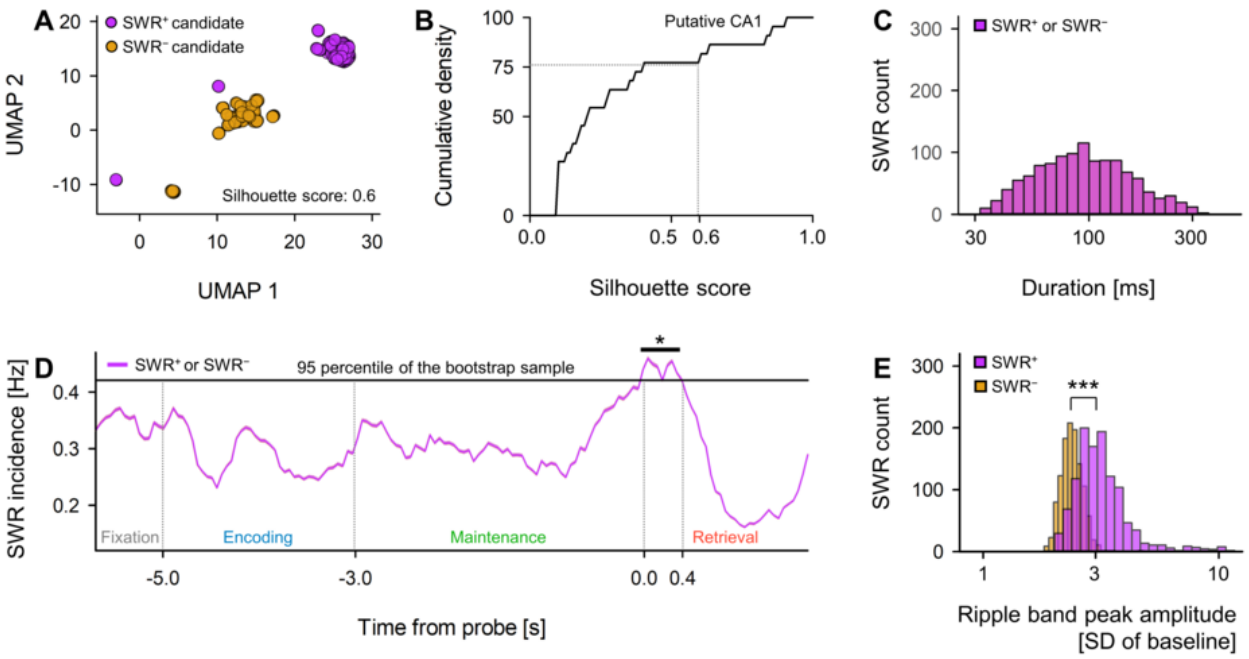


**Figure 4 – Detection of SWRs in Presumptive CA1 Regions**

***A.*** Two-dimensional UMAP (Uniform Manifold Approximation and Projection) [41] projection of multiunit spikes during $SWR^+$ candidates (*purple*) and $SWR^-$ candidates (*yellow*). ***B.*** Cumulative density plot shows silhouette scores, indicative of UMAP clustering quality, for hippocampal regions (see Table 2 for reference). Note that hippocampal regions with silhouette scores greater than 0.60 (equivalent to the $75^{th}$ percentile) were identified as possible CA1 regions. $SWR^+$ and $SWR^-$ candidates recorded from these speculative CA1 regions were respectively classified as $SWR^+$ and $SWR^-$ (*ns* = 1,170). ***C.*** The identical distributions of durations are presented for $SWR^+$ (*purple*) and $SWR^-$ (*yellow*), owing to their definitions (93.0 [65.4] ms, median [IQR]). ***D.*** SWR incidence for both $SWR^+$ (*purple*) and $SWR^-$ (*yellow*) obtained relative to the probe's timing is illustrated as a mean ±95% confidence interval. However, as the intervals may not be visible due to their narrow range, note that a significant increase in SWR incidence was detected during the initial 400 ms of the retrieval phase (0.421 [Hz], $*p < 0.05$, bootstrap test). ***E.*** The distributions of ripple band peak amplitudes for $SWR^-$ (*yellow*; 2.37 [0.33] SD of baseline, median [IQR]) and $SWR^+$ (*purple*; 3.05 [0.85] SD of baseline, median [IQR]) are delineated ($***p < 0.001$, the Brunner–Munzel test).

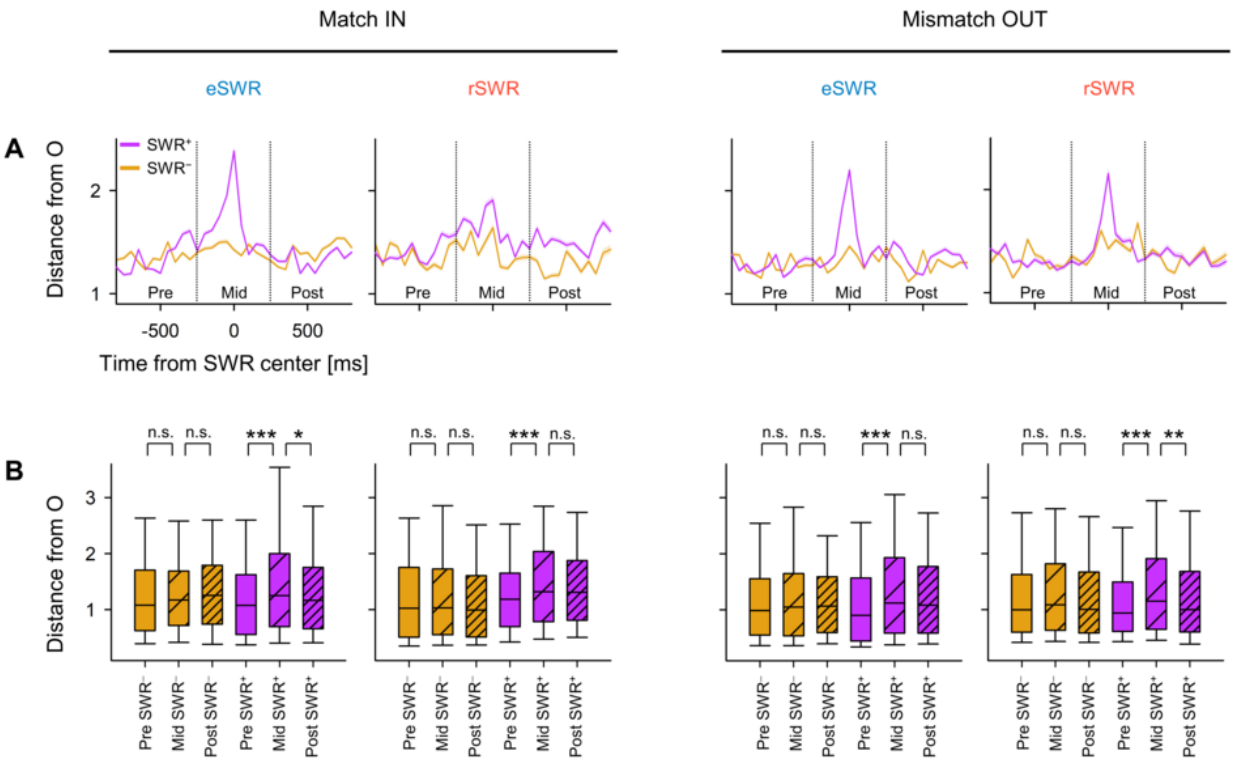


**Figure 5 – Transient Alterations in Neural Trajectory During SWR Events**

***A.*** Displayed is the distance from origin ($O$) of the peri-sharp-wave-ripple trajectory (mean ±95% confidence interval). The intervals may not be apparent due to their slender ranges. ***B.*** Shown is the distance from the origin ($O$) during pre-, mid-, and post-SWR periods ($^*p < 0.05$, $^{**}p < 0.01$, $^{***}p < 0.001$; assessed using the Brunner–Munzel test). Abbreviations: SWR, sharp-wave ripple events; eSWR, SWR during the encoding phase; rSWR, SWR while in the retrieval phase; $SWR^+$, positive SWR event; $SWR^-$, control events for $SWR^+$; pre-, mid-, or post-SWR denote the time intervals from −800 to −250 ms, from −250 to +250 ms, or from +250 to +800 ms, all relative to the center of the SWR.

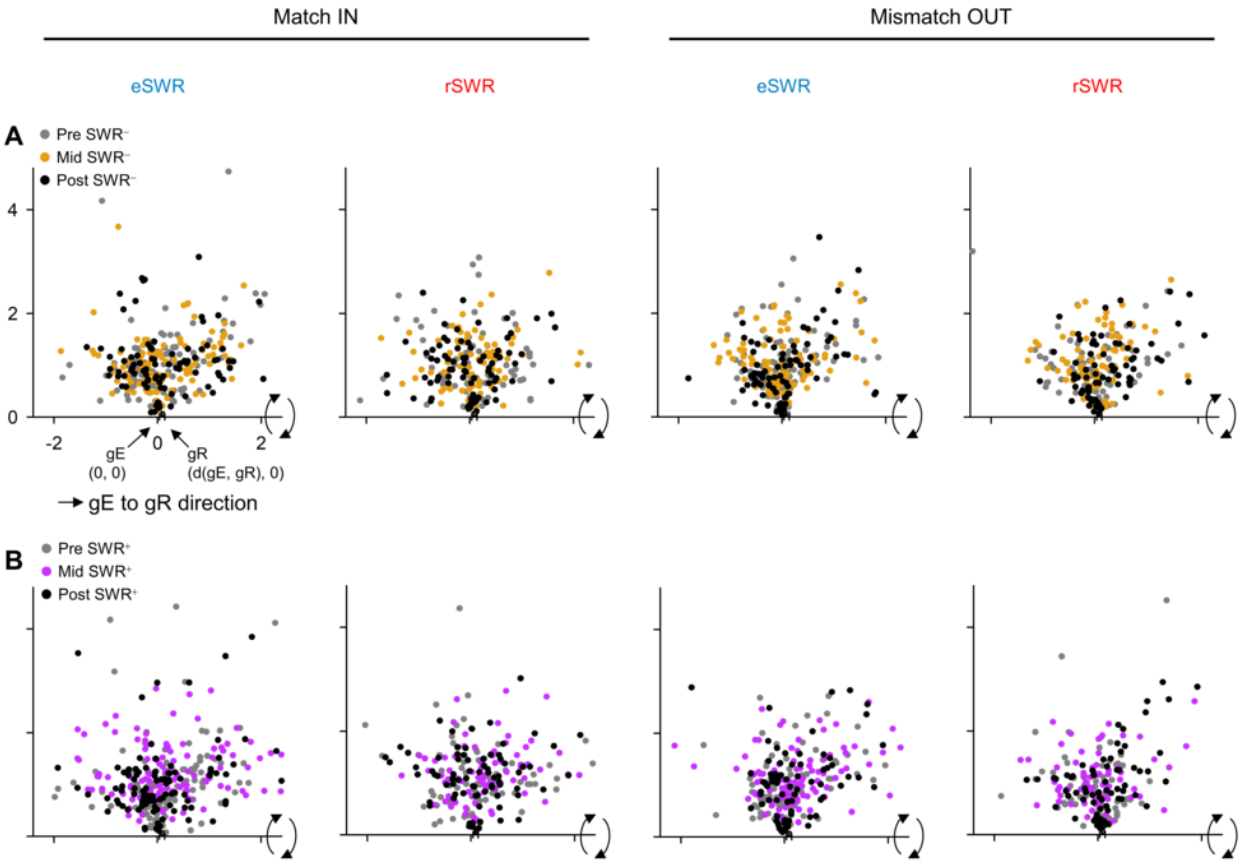


**Figure 6 – Visualization of Neural Trajectories during SWR in Two-Dimensional Spaces**

The panels display hippocampal neural trajectories during SWR as projected onto two-dimensional spaces. ***A.*** Indicates hippocampal neural trajectories pre-SWR$^-$ (*gray*), mid-SWR$^-$ (*yellow*), and post-SWR$^-$ (*black*). ***B.*** Represents the equivalents for SWR$^+$ as opposed to SWR$^-$. The $\|g_E g_R\|$ varied among sessions. The projection was applied in the following manner: First, a linear transformation positioned $g_E$ at the origin $O$ (0,0), and $g_R$ at ($\|g_E g_R\|$, 0). The point cloud was then rotated around the $g_E g_R$ axis (equivalent to the x axis) for fitting into two-dimensional spaces. Therefore, within these two-dimensional spaces, both the distances from $O$ and the angles preserved the original makeup of the $g_E g_R$ axis from the original three-dimensional spaces. Abbreviations: SWR signifies sharp-wave ripple events; eSWR denotes SWR during the encoding phase; rSWR indicates SWR during the retrieval phase; SWR$^+$, marks an SWR event; SWR$^-$ refers to control events for SWR$^+$; pre-SWR, mid-SWR, or post-SWR, reference the time intervals from −800 to −250 ms, from −250 to +250 ms, or from +250 to +800 ms from the center of SWR.

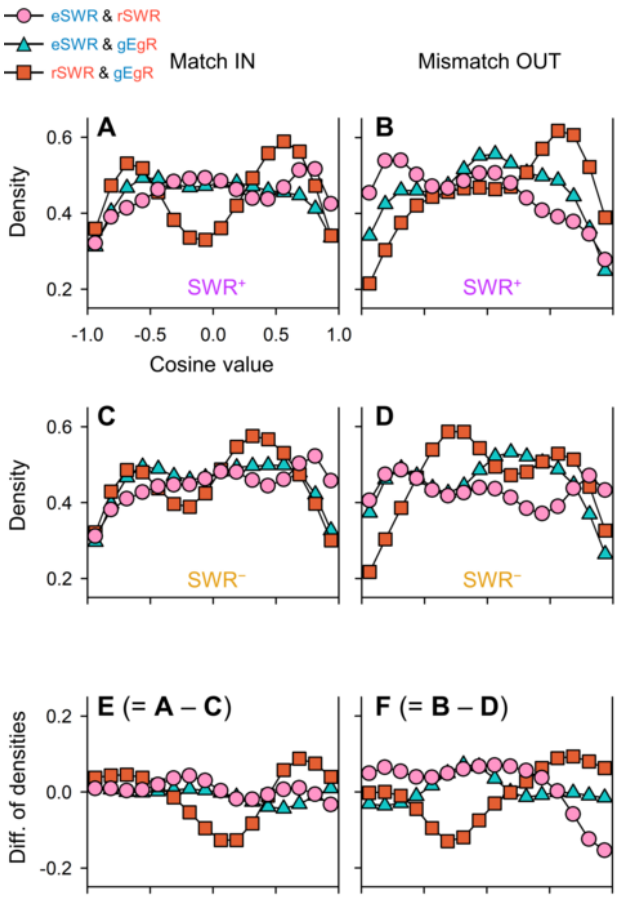


**Figure 7 – Directions of Neural Trajectories during SWRs Based on Encoding and Retrieval States**

***A–B*** Kernel density estimation (KDE) distributions of $\overrightarrow{\mathrm{eSWR}^{+}} \cdot \overrightarrow{\mathrm{rSWR}^{+}}$ (*pink circles*), $\overrightarrow{\mathrm{eSWR}^{+}} \cdot \overrightarrow{\mathrm{g_E g_R}}$ (*blue triangles*), and $\overrightarrow{\mathrm{rSWR}^{+}} \cdot \overrightarrow{\mathrm{g_E g_R}}$ (*red rectangles*) in Match In (*A*) and Mismatch OUT tasks (*B*). ***C–D*** Present the corresponding distributions of $\mathrm{SWR}^{-}$ instead of those of $\mathrm{SWR}^{+}$ in *A* and *B*. ***E–F*** Depict the differences in the distributions of $\mathrm{SWR}^{+}$ and $\mathrm{SWR}^{-}$, illuminating the SWR components ($E = C - A$; $F = D - B$). Note the biphasic distributions of $\overrightarrow{\mathrm{rSWR}^{-}} \cdot \overrightarrow{\mathrm{g_E g_R}}$, suggesting fluctuations between the encoding and retrieval states during the Sternberg task. Moreover, inverse directionality between $\overrightarrow{\mathrm{eSWR}^{+}}$ and $\overrightarrow{\mathrm{rSWR}^{+}}$ was observed (*pink circles*) in the Mismatch OUT task, but not in the Match IN task ***E–F***). Finally, shifts from the retrieval to encoding states were evident in the SWR components in both the Match IN and Mismatch OUT tasks (*red rectangles* in *E* and *F*).